Volume 14
Number 38
14 October 2022
Pages 13847-14306

Nanoscale

rsc.li/nanoscale

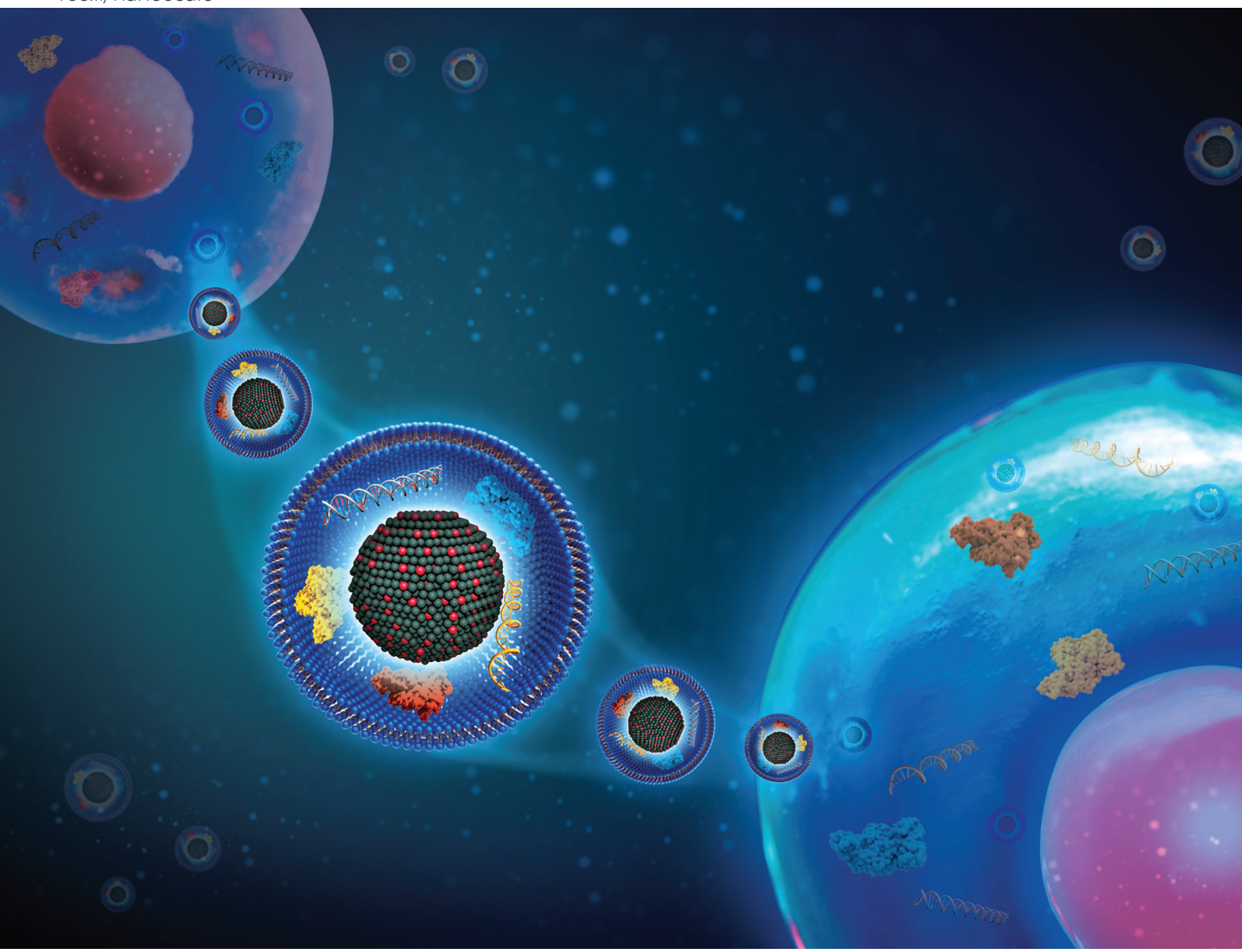

ISSN 2040-3372

ROYAL SOCIETY OF CHEMISTRY

COMMUNICATION
Sang Hwan Nam, Yung Doug Suh, Kang Taek Lee *et al.*
Visualization of intercellular cargo transfer using upconverting nanoparticles

NCNST

Nanoscale

COMMUNICATION

View Article Online
View Journal | View Issue

Cite this: *Nanoscale*, 2022, **14**, 14008

Received 12th April 2022,
Accepted 11th August 2022

DOI: 10.1039/d2nr01999j

rsc.li/nanoscale

Visualization of intercellular cargo transfer using upconverting nanoparticles†

Yeongchang Goh, ‡[a] Jongwoo Kim, ‡[b] Hye Sun Park, ‡[c] Taeyoung Jung,[a,b] Kwan Soo Hong,[c,d] Sang Hwan Nam, *[b] Yung Doug Suh *[e,f] and Kang Taek Lee *[a]

Cell–cell communication is important for cellular differentiation, organ function, and immune responses. In intercellular communication, the extracellular vesicles (EVs) play a significant role in delivering the cargo molecules such as genes, proteins, and enzymes, to regulate and control the ability of the recipient cells. In this study, the observation of intercellular cargo transfer *via* dual-colour imaging using upconverting nanoparticles (UCNPs) has been demonstrated. Using this technique, the intercellular transport *via* contact-dependent and contact-independent signaling in live HeLa cells was clearly visualized with real-time, long-term single-vesicle tracking. Furthermore, it was demonstrated that the endocytosed UCNPs can be transmitted with the encapsulation of EVs labelled with fluorescent proteins.

Introduction

Cell–cell communication is crucial for cell development, tissue interactions, and immune response.[1] The intercellular communication with the transmission of biochemical signals can be contact-dependent through cell surface molecules or contact-independent through the secretion of extracellular vesicles (EVs), which are cell-derived membrane vesicles released from cells.[2–4] Intercellular communication *via* secreted EVs has been firmly established for more than two decades, emphasizing the importance of functional cargos, formed as proteins and nucleic acids transferred from one cell to another in physiological and pathological processes.[4–6]

To understand cell–cell communication *via* EVs, the visualization of EVs using fluorescence microscopy has been intensively investigated. The internalization and trafficking of exosomes were demonstrated using lipophilic fluorescent dye using real-time fluorescence microscopy.[7] The exchange and uptake of EVs between different types of cells were visualized using multiplexed live-cell imaging based on palmitoylated fluorescent proteins.[8] The endocytosis of EVs and release of their cargo were identified through the expression of fluorescent proteins using correlative light and electron microscopy.[3]

However, fluorescent proteins and/or organic fluorophores undergo photobleaching, which restricts the imaging time. Therefore, tracking cargo mediated by EVs in recipient cells based on the labelling of fluorescent proteins on EV membrane proteins, such as CD63, remains challenging. As a bioimaging probe, upconverting nanoparticles (UCNPs) have been widely employed because of their various advantages, including high photostability without photobleaching or photoblinking that facilitates long-term tracking, uniform size and intensity, low cytotoxicity owing to near-infrared (NIR) excitation, no autofluorescence because of large anti-Stokes shift, and multiplexed emission with different activator doping under a single light source.[9–18] UCNPs functionalized with poly(ethylene glycol) (PEG), which are photostable for tens of hours,[19] can be internalized into a cell through endocytosis and moved in a vesicle as a cargo along the microtubule by motor proteins.[13] Additionally, the cellular interaction of the PEGylated UCNPs, including endocytosis, intracellular transport, and exocytosis was reported in living HeLa cells.[14] Therefore, it can be hypothesized that the PEGylated UCNPs exocytosed from cells have the form of EVs, in particular exosomes.

In this study, the intercellular cargo transfer between HeLa cells was visualized using multiplexed live-cell imaging based on PEGylated UCNPs as cargos. The approach of two cells fol-

[a]*Department of Chemistry, Gwangju Institute of Science and Technology (GIST), Gwangju, South Korea. E-mail: ktlee@gist.ac.kr*
[b]*Laboratory for Advanced Molecular Probing (LAMP), Korea Research Institute of Chemical Technology (KRICT), Daejeon, South Korea*
[c]*Research Center for Bioconvergence Analysis, Korea Basic Science Institute (KBSI), Cheongju, South Korea*
[d]*Graduate School of Analytical Science and Technology (GRAST), Chungnam National University, Daejeon, South Korea*
[e]*Department of Chemistry, Ulsan National Institute of Science and Technology (UNIST), Ulsan, South Korea*
[f]*School of Energy and Chemical Engineering, Ulsan National Institute of Science and Technology (UNIST), Ulsan, South Korea*
†Electronic supplementary information (ESI) available: Supplementary Fig. S1–S5. See DOI: https://doi.org/10.1039/d2nr01999j
‡These authors contributed equally.

lowed by cell adhesion and contact-dependent cargo transfer between the cells was observed using single-particle tracking (SPT). It was demonstrated that the endocytosed UCNPs can be transmitted in the form of EV with fluorescent labelling of the EV membrane, and their membrane moves with the cargo rather than fusing with the plasma membrane in the recipient cell. This technique is a powerful tool for tracking cargo in live cells to monitor intercellular communication.

Results and discussion

Fig. 1 shows a schematic of intercellular particle transfer in live cells using UCNPs. The sizes of the synthesized Er^{3+}-doped UCNPs and Tm^{3+}-doped UCNPs were 26 and 27 nm, respectively (Fig. S1a and S1b†). The PEGylated Er^{3+}-doped UCNPs (Er-UCNPs) and PEGylated Tm^{3+}-doped UCNPs (Tm-UCNPs) showed well-dispersion stability (Fig. S2a and S2d†). The hydrodynamic diameter of Er-UCNPs and Tm-UCNPs were 40.2 nm and 36.7 nm, respectively (Fig. S2b and S2e†). Er-UCNPs and Tm-UCNPs were found to be have negative surface charges (Fig. S2c and S2f†). Er-UCNPs and Tm-UCNPs were excited by a single 980 nm laser, and their different emission bands, 650 nm for Er-UCNPs and 800 nm for Tm-UCNPs (Fig. S1c†), were separated using the imaging system. Er-UCNPs and Tm-UCNPs were internalized into two groups of HeLa cells, respectively (Fig. 1a). Subsequently, the Er-UCNP-incubated cells and Tm-UCNP-incubated cells were mixed and cultured (Fig. 1b). It is advantageous to introduce UCNPs without photobleaching or photoblinking for live-cell imaging, which facilitates the real-time monitoring of intercellular material transport in live cells for up to several tens of hours,[13–16,20–22] much longer than that of organic fluorophores[7,23] or fluorescent proteins.[8] The material transport between cells was observed *via* a home-built dual-colour imaging system (Fig. 1c and S3†), which enables long-term particle tracking and transfer between live cells using a single 980 nm laser and monitoring of cell migration. Approximately 6 h after the mixed incubation, most cells contained one type of internalized UCNPs, and no cells containing both Er-UCNPs and Tm-UCNPs were detected (Fig. S4a†), while some cells contained both Er-UCNPs and Tm-UCNPs after approximately 12 h after the mixed incubation (Fig. S4b†). This indicates that the UCNPs internalized in the original cells moved to other cells.

Based on this observation, the imaging and tracking of UCNPs was performed between 6 and 12 h after the mixed incubation (Fig. 2). Photoluminescence (PL) images of the two types of UCNPs were obtained every second, and bright-field images were obtained every 10 min. The transfer of UCNPs between two HeLa cells from 10 h 20 min to 10 h 40 min post-mixed-incubation is shown in Video S1.† Before the UCNP transfer, only one type of UCNPs was found in individual cells, and two cells, Cell A internalized by Er-UCNPs and Cell B internalized by Tm-UCNPs, were far from each other at 8 h post-mixed-incubation (Fig. 2a). Cells A and B gradually came closer (Fig. S5†), which may be attributed to cell migration through chemotaxis,[24] probably because they move along the concentration gradient of EVs secreted by the counterparts.[25–27] The two cells started to establish cell–cell junctions (Fig. 2b) and then formed stable interfaces after 1 h (Fig. 2c). Two Er-UCNPs (particles P and Q) in Cell A moved to the cell boundary (Fig. 2d) after 12 min from the cell adhesion. Approximately 6 min later, particles P and Q that crossed the boundary moved to Cell B (Fig. 2e and f). Additionally, cell division was observed in Cell C during the continuous illumination of a 980 nm laser (Fig. 2). This indicates that the irradiation with the laser at

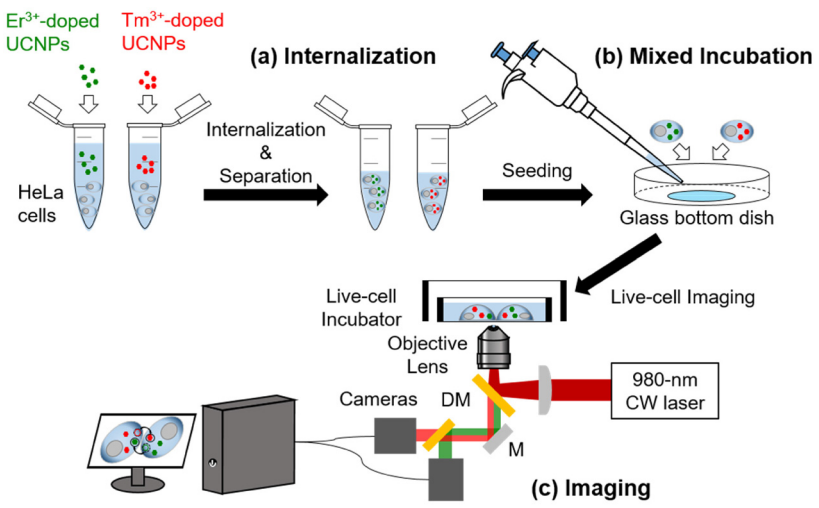

Fig. 1 Schematic of an experiment for the long-term, real-time observation of intercellular cargo transport between HeLa cells. (a) Two types of PEGylated UCNPs (Er-UCNPs and Tm-UCNPs) were internalized in two independent batches of HeLa cells for 30 min. Next, UCNPs not internalized are removed *via* centrifugation. (b) Two batches were mixed on a glass-bottom dish. (c) UCNPs internalized into HeLa cells were excited using a 980 nm continuous-wave (CW) laser; the emissions from two types of UCNPs were separated by dichroic mirrors (DM) and collected simultaneously every second by two cameras.

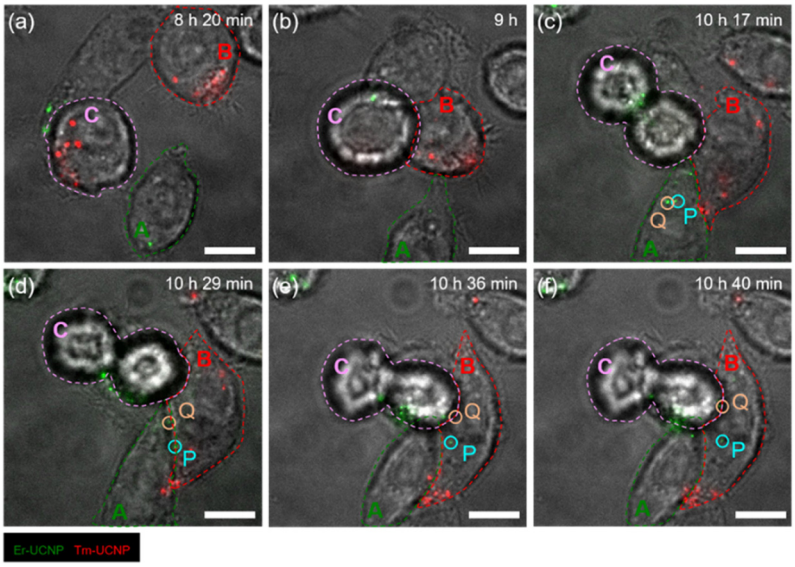

Fig. 2 Cell migration and material transfer *via* cell–cell communication in living HeLa cells. Images of Er-UCNPs, Tm-UCNPs, and bright-field are overlaid. Cells A and B are originally incubated by Er-UCNPs and Tm-UCNPs, respectively. Cell C shows cell division, indicating very low phototoxicity during continuous irradiation. Particle P (blue circle) and particle Q (yellow circle) show that the Er-UCNPs were originally in Cell A and transferred to Cell B. Photoluminescence (PL) images of UCNPs were taken every second, and the bright-field images were taken every 10 min. Timestamps represent the time after the mixed incubation. Scale bars represent 10 μm. Video from 10 h 20 min to 10 h 40 min is also available in Video S1.†

several kW cm^{-2} of the live cells was not phototoxic, which is consistent with the previous reports.[13,20,21] Furthermore, the vesicles containing Tm-UCNPs in Cell B moved near Cell A (Fig. 2). Material transfer from Cell A to Cell B strongly suggests juxtacrine signalling of contact-dependent cell–cell communication to pass signalling cargos directly between cells.[1]

To confirm whether the transferred Er-UCNPs were in the recipient cell (Cell B) in Fig. 2, SPT and mean-square displacement (MSD) analysis were used (Fig. 3).[12,28–31] The MSD plot is described by the following equation:

$$\mathrm{MSD}\,(n\tau) = \frac{1}{N-n} \sum_{i=1}^{N-n}\left[(x((i+n)\tau) - x(i\tau))^2 + (y((i+n)\tau) - y(i\tau))^2\right] \quad (1)$$

where τ is the acquisition time, and N is the total number of frames. As a function of time, $t = n\gamma$, the motion is described by the following equation:

$$\mathrm{MSD}(t) = 4Dt^{\gamma} \quad (2)$$

where D is the diffusion constant, and γ is the exponent.[31] The motion is classified into two categories by the exponent: sub-diffusion affected by cellular crowding or molecular interactions when $\gamma < 1$ and super-diffusion, such as active transport, when $\gamma > 1$. Trajectory P1 in Fig. 3b shows the movement of particle P in Fig. 2 for approximately 2 min from 10 h 30 min post-mixed incubation. The exponent of Trajectory P1 is 1.12 during the tracking, which mainly indicates active transport motion, implying that the vesicles are controlled by

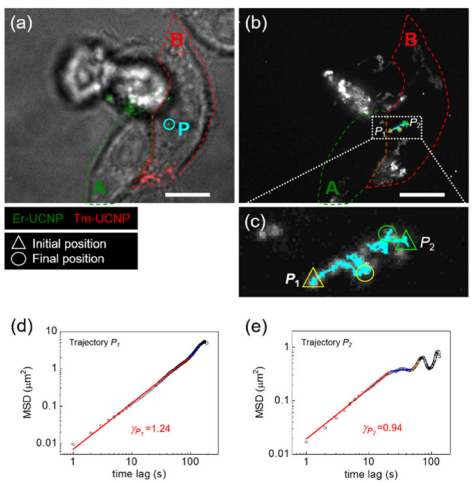

Fig. 3 Single-particle tracking (SPT) analysis of the transferred UCNPs in living HeLa cells. (a) Snapshot image at 10 h 40 min after mixed incubation in Fig. 2. Boundaries of Cells A (containing Er-UCNPs) and B (containing Tm-UCNPs) are indicated by red and green dashed lines, respectively. (b) Projection image of UCNPs is shown in the video from 10 h 30 min to 10 h 40 min post-mixed-incubation. (c) Magnified image of the white box in (b). Trajectories of UCNPs are separated into two: P1 and P2. (d and e) mean-square displacement (MSD) plots and their exponent values of Trajectories P1 and P2 as 1.24 and 0.94, which indicate active transport and sub-diffusion, respectively. Scale bars represent 10 μm.

the motor proteins of the recipient, *i.e.*, Cell B. After the motion along Trajectory P1, the exponent of Trajectory P2 is 0.94, which shows sub-diffusion motion.[31] From Fig. 3c, the final position of Trajectory P2 is negligibly different from the

initial position. The MSD analysis for Particle Q in Fig. 2 are shown in Fig. S6.† Similarly, Trajectories Q1 and Q2 in Fig. S6† show the exponent values as 0.95 (sub-diffusion motion) and 1.13 (active transport), respectively. MSD analysis shows that the transferred Er-UCNPs were regulated by the recipient cell. This reveals more clearly that the transferred Er-UCNPs were in Cell B, one of the Tm-UCNP-incubated cells. Their motion is very similar to the movement of UCNPs internalized by endocytosis inside vesicles along the microtubule by motor proteins.[13]

To assess whether the UCNP cargos are transferred to the recipient cell with the surface protein of EVs in contact-independent cell–cell communications, the HeLa cells had been transduced with a lentivirus vector encoding, red fluorescent protein (RFP) conjugated with CD63, a tetraspanin highly enriched in the intraluminal vesicles and EVs.[32] Fig. 4 shows the *z*-projection of three-dimensional images of a CD63-RFP-expressing HeLa cell (Fig. 4a and b) initially incubated with Tm-UCNPs and a wild-type HeLa cell (Fig. 4c and d) initially incubated with Er-UCNPs at 24 h after mixed incubation of the two groups of HeLa cells, obtained *via* super-resolution radial fluctuation (SRRF).[33] The fluorescence of RFP was distributed in the CD63-RFP-expressing HeLa cell (Fig. 4a), indicating that the RFP was successfully expressed in HeLa cells. The co-localization of Tm-UCNPs and RFP in the CD63-RFP-expressing cell (Fig. 4b) reveals that the existing Tm-UCNPs were internalized in intraluminal vesicles or that the Tm-UCNPs were endocytosed while being internalized in EVs from other CD63-RFP-expressing HeLa cells. Additionally, Er-UCNPs were evident in the CD63-RFP-expressing HeLa cell (Fig. 4b), suggesting the internalization of the cargo from the wild-type HeLa cells *via* paracrine signalling, which is a type of cell–cell communication without cell–cell contact.[1] In the wild-type HeLa cells (Fig. 4c and d), the RFP fluorescence indicates that EVs exocytosed from CD63-RFP-expressing HeLa cells were not fused with the plasma membrane or endosome membrane of the recipient cell, which is consistent with the EV internalization *via* endocytosis and the suppressed release of EV contents due to the neutralization of endosomal pH and accumulation of cholesterol in endosomes.[3] Furthermore, Tm-UCNPs co-localized with CD63-RFPs were observed in the wild-type HeLa cells (Fig. 4c), indicating that the cargos exocytosed from a CD63-RFP-expressing HeLa cell and transferred to the wild-type HeLa cell were encapsulated by the EVs.

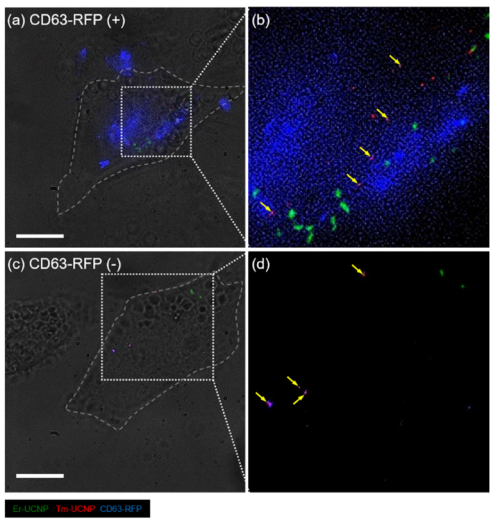

Fig. 4 Super-resolution radial fluctuation (SRRF) images of CD63-RFP-expressed and wild-type HeLa cells containing UCNPs. (a) Merged image of Er-UCNPs, Tm-UCNPs, and CD63-RFP in CD63-RFP expressed HeLa cells. White dotted line shows the cell boundary. (b) Magnified image of the white box in (a) without the bright-field image. (c) Merged image of Er-UCNPs, Tm-UCNPs, and CD63-RFP in wild-type HeLa cells. White dotted line shows the cell boundary. (d) Magnified image of the white-dashed box in (c) without the bright-field image. Yellow dots marked with the yellow arrows show the co-localization of Tm-UCNPs with CD63-RFP. Scale bars represent 10 μm.

Conclusions

In this study, a method for real-time monitoring based on the dual-colour imaging of PEGylated UCNPs as cargos was proposed to visualize intercellular communication. Using this technique, the transport of intercellular materials was monitored for several hours through SPT in live cells, without chemical- or phototoxicity. It was demonstrated that cargo transport between live cells that occurred in contact or at long distances could be tracked at the level of a single vesicle. Additionally, it was confirmed that the membrane and cargo of EVs could be distinguished through the fluorescence imaging of the membrane proteins of EVs and PL imaging of UCNPs.

This technique, combined with fluorescence imaging will help elucidate the fundamental roles of cells and their functions within their communities. Additionally, nanoparticle-containing EVs can contribute to fundamental studies of EVs, such as the quantitative analysis of EVs depending on the cell type, and environment using PL emitted from UCNPs as their cargo. Furthermore, this technique is expected to not only strengthen the understanding of biochemical events behind intercellular interaction, but also to provide an opportunity for developing next-generation cell-based therapeutics.

Materials and methods

Synthesis of UCNPs

UCNPs of β-$NaYF_4$:20 mol% Yb^{3+},2 mol% Er^{3+} were synthesized according to previously reported methods.[34] Yttrium acetate hydrate (0.312 mmol), ytterbium acetate hydrate (0.08 mmol), erbium acetate hydrate (0.008 mmol) were dissolved in deionized water. The solution was added to a mixture of 3 mL of oleic acid (OA) and 7 mL of 1-octadecene (1-ODE) in a 50 mL two-neck round-bottom flask and heated to 150 °C with stirring for 30 min. After cooling, 1.6 mmol of ammonium fluoride and 1 mmol of sodium hydroxide dis-

solved in methanol were added to the flask and heated to 50 °C with stirring for 30 min. The solution was heated to 100 °C under vacuum with stirring for 30 min to remove any residual solvent. Subsequently, the solution was heated to 290 °C and maintained at 290 °C under argon for 2 h. After cooling, the UCNPs were precipitated through the addition of ethanol. After centrifugation, the nanoparticles were dispersed in hexane. In the case of β-$NaYF_4$:20 mol% Yb^{3+},1 mol% Tm^{3+} UCNPs, 0.316 mmol of yttrium acetate hydrate, 0.08 mmol of ytterbium acetate hydrate, and 0.004 mmol of thulium acetate hydrate were used instead.

PEGylation of UCNPs and their characterization

UCNPs encapsulated in PEG-phospholipids were synthesized as previously reported. The UCNPs (2 mg) in chloroform were slowly added to an aqueous solution of 1,2-dipalmitoyl-*sn-glycero*-3-phosphoethanolamine-*N*-[methoxy(polyethylene glycol)-2000] (mPEG; Nanocs, Inc.) during tip sonication (Branson Sonifier, USA) for 3 min, and the emulsion mixture was vigorously vortexed and stirred for 2 h. After evaporating the solvent, UCNPs were purified *via* centrifugation and dispersed in deionized water. The PEGylated UCNPs were characterized by high-resolution transmission electron microscopy (HR-TEM; JEM-1400 Plus, JEOL, Japan). Their particle size distribution and surface zeta potential were analysed using a particle size analyser (NanoZS, Malvern Instruments LTD, UK).

Internalization of UCNPs into HeLa cells

HeLa cells were cultured in Dulbecco's modified Eagle's medium (DMEM) with 10% heat-inactivated fetal bovine serum and 1% penicillin–streptomycin at 37 °C in a 5% CO_2 incubator. HeLa cells were seeded in a T25 culture flask and cultured for 2 d. HeLa cells were then detached using trypsin ethylenediaminetetraacetic acid (EDTA) at a cell density of 10^5 cells per mL. PEGylated Er- and Tm-UCNPs (5 mg mL^{-1}, 20 μL) were separately injected into the culture medium and incubated for 30 min. After incubation, UCNPs that were not internalized into the cells but dispersed in the culture medium were removed *via* centrifugation. After mixing the two types of HeLa cells containing each type of UCNPs, the mixed HeLa cells were seeded on a 25Φ glass-bottom dish and incubated for 6 h in a cell incubator.

Observation of intercellular material transport using dual-colour imaging

HeLa cells were placed on an inverted microscope (IX71, Olympus) equipped with a live-cell incubator (Chamlide TC, Live Cell Instrument). The sample was excited by a 980 nm laser diode (AC1401-0600-0980-SM, Gooch & Housego) for PL imaging. To collect the emission from Er-UCNPs and Tm-UCNPs separately, bandpass filters (FF01-660/13, Semrock for Er-UCNPs; F1 in Fig. S3† and FF01-800/12, Semrock for Tm-UCNPs; F2 in Fig. S3†) were used. For dividing the dual-colour emission, a 785 nm long-pass dichroic beamsplitter (LPD02-785RU, Semrock) was used. Images were captured using two electron-multiplying charge-coupled device (EMCCD) cameras (DU-888E-C00-#BV, Andor for Er-UCNPs; DU-888D-C00-#EX, Andor for Tm-UCNPs). PL images of UCNPs were obtained every second, and bright-field images of HeLa cells were obtained every 10 min.

Expression of RFP in HeLa cells

HeLa cells were seeded in a 6-well plate (SPL) for 24 h at a concentration of 5×10^5 cells per mL. RFP was transfected with HeLa cells and fused to CD63 tetraspanin using a lentivirus vector (pCT-CD63-RFP, System Biosciences) with a transfection reagent (Lipofectamine 3000 Transfection Reagent, ThermoFisher Scientific). After 48 h of incubation, CD63-RFP-expressing HeLa cells with Tm-UCNPs and wild-type HeLa cells with Er-UCNPs were mixed on a glass-bottom dish. After 24 h of mixing, the sample was fixed with a 5% paraformaldehyde solution.

SRRF imaging

SRRF imaging was performed at a high spatial resolution of 50 to 150 nm. A single SRRF image was reconstructed with each 100 identical UCNPs and RFP images using the SRRF microscopy software (Oxford Inc.). Scanning through the *z*-axis was controlled using a piezo objective scanner for a three-dimensional (3-D) SRRF. The sample was scanned with at a depth of 500 nm along the *z*-axis, with a total scanning range of 17 500 nm. The acquisition time for the 3-D SRRF image was approximately 1 s. The 3-D scanning was performed using the 3-D piezo objective scanner with a home-made LabVIEW software. For the dual-colour imaging of Er-UCNPs and Tm-UCNPs, two filters, 600/50 bandpass filter (ET600/50, Chroma Technology) and 811/80 bandpass filter (ET811/80, Chroma Technology), were used, respectively (Fig. S3†). The analysis of the co-localization of the UCNPs and RFP was performed using the ImageJ software.

Conflicts of interest

There are no conflicts to declare.

Acknowledgements

K. T. L. acknowledges support from the National Research Foundation of Korea (NRF) grant funded by the Ministry of Science and ICT (2021R1A2C2010557) and support by GIST Research Institute (GRI) grant funded by the GIST in 2022. Y. D. S. and S. H. N. acknowledges support by the Global Research Laboratory (GRL) program through the National Research Foundation of Korea (NRF) funded by the Korea Government (MSIT) (2016911815), and KRICT (KK2261-12). K. S. H. and H. S. P acknowledges support from the National Research Foundation of Korea (NRF) grant funded by the Korea Government (MIST) (2020R1A2C2012011) and a grant from KBSI (C210400).

References

1 E. Armingol, A. Officer, O. Harismendy and N. E. Lewis, *Nat. Rev. Genet.*, 2021, **22**, 71–88.
2 T. J. Bechtel, T. Reyes-Robles, O. O. Fadeyi and R. C. Oslund, *Nat. Chem. Biol.*, 2021, **17**, 641–652.
3 B. S. Joshi, M. A. de Beer, B. N. G. Giepmans and I. S. Zuhorn, *ACS Nano*, 2020, **14**, 4444–4455.
4 R. C. Paolicelli, G. Bergamini and L. Rajendran, *Neuroscience*, 2019, **405**, 148–157.
5 D. S. Chulpanova, K. V. Kitaeva, V. James, A. A. Rizvanov and V. V. Solovyeva, *Front. Immunol.*, 2018, **9**, 1534.
6 M. Tkach and C. Théry, *Cell*, 2016, **164**, 1226–1232.
7 T. Tian, Y.-L. Zhu, F.-H. Hu, Y.-Y. Wang, N.-P. Huang and Z.-D. Xiao, *J. Cell. Physiol.*, 2013, **228**, 1487–1495.
8 C. P. Lai, E. Y. Kim, C. E. Badr, R. Weissleder, T. R. Mempel, B. A. Tannous and X. O. Breakefield, *Nat. Commun.*, 2015, **6**, 7029.
9 H. S. Park, J. Kim, M. Y. Cho, Y. J. Cho, Y. D. Suh, S. H. Nam and K. S. Hong, *ACS Appl. Mater. Interfaces*, 2020, **12**, 49362–49370.
10 A. H. All, X. Zeng, D. B. L. Teh, Z. Yi, A. Prasad, T. Ishizuka, N. Thakor, Y. Hiromu and X. Liu, *Adv. Mater.*, 2019, **31**, 1803474.
11 X. Zeng, S. Chen, A. Weitemier, S. Han, A. Blasiak, A. Prasad, K. Zheng, Z. Yi, B. Luo, I.-H. Yang, N. Thakor, C. Chai, K.-L. Lim, T. J. McHugh, A. H. All and X. Liu, *Angew. Chem., Int. Ed.*, 2019, **58**, 9262–9268.
12 F. Wang, S. Wen, H. He, B. Wang, Z. Zhou, O. Shimoni and D. Jin, *Light: Sci. Appl.*, 2018, **7**, 18007.
13 S. H. Nam, Y. M. Bae, Y. I. Park, J. H. Kim, H. M. Kim, J. S. Choi, K. T. Lee, T. Hyeon and Y. D. Suh, *Angew. Chem., Int. Ed.*, 2011, **50**, 6093–6097.
14 Y. M. Bae, Y. I. Park, S. H. Nam, J. H. Kim, K. Lee, H. M. Kim, B. Yoo, J. S. Choi, K. T. Lee, T. Hyeon and Y. D. Suh, *Biomaterials*, 2012, **33**, 9080–9086.
15 G. Chen, H. Qiu, P. N. Prasad and X. Chen, *Chem. Rev.*, 2014, **114**, 5161–5214.
16 Y. I. Park, K. T. Lee, Y. D. Suh and T. Hyeon, *Chem. Soc. Rev.*, 2015, **44**, 1302–1317.
17 A. Gnach, T. Lipinski, A. Bednarkiewicz, J. Rybka and J. A. Capobianco, *Chem. Soc. Rev.*, 2015, **44**, 1561–1584.
18 G. Huang, Y. Zhu, S. Wen, H. Mei, Y. Liu, D. Wang, M. Maddahfar, Q. P. Su, G. Lin, Y. Chen and D. Jin, *Nano Lett.*, 2022, **22**, 3761–3769.
19 J.-C. Boyer, M.-P. Manseau, J. I. Murray and F. C. van Veggel, *Langmuir*, 2010, **26**, 1157–1164.
20 Y. Goh, Y. H. Song, G. Lee, H. Bae, M. K. Mahata and K. T. Lee, *Phys. Chem. Chem. Phys.*, 2018, **20**, 11359–11368.
21 H. L. Jo, Y. H. Song, J. Park, E. J. Jo, Y. Goh, K. Shin, M. G. Kim and K. T. Lee, *Nanoscale*, 2015, **7**, 19397–19402.
22 Y. I. Park, H. M. Kim, J. H. Kim, K. C. Moon, B. Yoo, K. T. Lee, N. Lee, Y. Choi, W. Park, D. Ling, K. Na, W. K. Moon, S. H. Choi, H. S. Park, S.-Y. Yoon, Y. D. Suh, S. H. Lee and T. Hyeon, *Adv. Mater.*, 2012, **24**, 5755–5761.
23 A. M. Booth, Y. Fang, J. K. Fallon, J.-M. Yang, J. E. K. Hildreth and S. J. Gould, *J. Cell Biol.*, 2006, **172**, 923–935.
24 D. Dormann and C. J. Weijer, *Curr. Opin. Genet. Dev.*, 2003, **13**, 358–364.
25 A. Lo Cicero, P. D. Stahl and G. Raposo, *Curr. Opin. Cell Biol.*, 2015, **35**, 69–77.
26 M. Simons and G. Raposo, *Curr. Opin. Cell Biol.*, 2009, **21**, 575–581.
27 M. A. Garcia, W. J. Nelson and N. Chavez, *Cold Spring Harbor Perspect. Biol.*, 2018, **10**, a029181.
28 M. J. Saxton, *Biophys. J.*, 1997, **72**, 1744–1753.
29 M. J. Saxton, *Nat. Methods*, 2008, **5**, 671–672.
30 X. Michalet, *Phys. Rev. E: Stat., Nonlinear, Soft Matter Phys.*, 2010, **82**, 041914.
31 C. Manzo and M. F. Garcia-Parajo, *Rep. Prog. Phys.*, 2015, **78**, 124601.
32 C. Théry, *et al.*, *J. Extracell. Vesicles*, 2018, **7**, 1535750.
33 S. Culley, K. L. Tosheva, P. Matos Pereira and R. Henriques, *Int. J. Biochem. Cell Biol.*, 2018, **101**, 74–79.
34 F. Wang, R. Deng and X. Liu, *Nat. Protoc.*, 2014, **9**, 1634–1644.